Journal of Materials Chemistry A

Accepted Manuscript

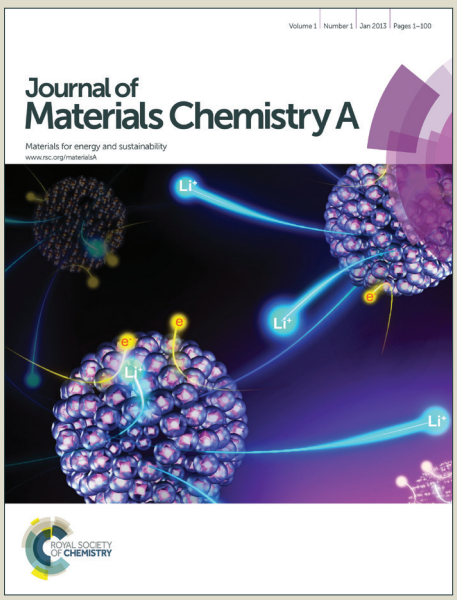

ROYAL SOCIETY OF CHEMISTRY

www.rsc.org/materialsA

Journal of Materials Chemistry A

ARTICLE

Nano-structural changes in Li-ion battery cathode during cycling revealed by FIB-SEM serial sectioning tomography

Received 00th January 20xx,
Accepted 00th January 20xx

DOI: 10.1039/x0xx00000x

www.rsc.org/

Bohang Song,[a,†] Tan Sui,[a] Siqi Ying,[a] Liu Li,[b] Li Lu,[b] Alexander M. Korsunsky[a,*]

The growing demand for reliable, durable electrical energy systems to power electric and hybrid vehicles motivates worldwide efforts aimed at developing high-energy, high-power density batteries. One of the obstacles to widespread industry adoption is the lack of profound understanding and the ability to monitor and control the long-term degradation and capacity fading observed in these systems. Focused Ion Beam-Scanning Electron Microscopy (FIB-SEM) serial sectioning is used to reconstruct the evolution of the three-dimensional structure of Li-ion battery electrodes during extended cycling. High resolution imaging reveals microstructural information at the level of the composite framework consisting of the spheroidal micro-particles of active material held together by the polymer matrix. The evolution of damage within the micro-particles of the active material can be seen in the form of voiding, cracking and ultimate fragmentation. In particular, when spherical micro-particles of Li-rich layered oxides are used as cathode, it is found that the extent of fragmentation varied in the direction of Li^+ diffusion current from the particle depth inwards. We use a simple model of the strain and strain gradient effects of Li^+ transient diffusion within the electrode to identify the driving force for particle fragmentation, and discuss the implication of these results.

Introduction

Ever since the successful commercialization of lithium-ion batteries (LIBs) in 1991, efforts have been directed at improving such aspects of battery performance as energy and power density, durability, safety, etc. Despite the conceptual agreement on the fundamentals of battery degradation, lack of detailed understanding of the hierarchical, multi-scale mechanisms responsible for capacity fading continues to hinder the development of the next-generation LIBs. To characterise the damage mechanisms operating at different scales, various analytical techniques have been utilized. For example, high-resolution transmission electron microscopy (HRTEM) has been widely applied to cycled particles of all types of electrode materials, revealing micro-cracks found at the crystal surface,[1] local phase transformation that manifests itself in atomic re-arrangement,[2,3] and material densification.[4] Inductively coupled plasma atomic emission spectroscopy (ICP-AES) and energy-dispersive X-ray spectroscopy (EDX) were applied to reveal the dissolution of transition metals due to the electrochemical cycling effects.[5-7] Powder X-ray diffraction (XRD) revealed a significant lattice unit cell volume change and structural breakdown as a result of (de)intercalation of Li.[8] Electrochemical impedance spectroscopy (EIS) proved that a gradual increase in the internal resistance of the electrodes takes place due to the formation of a solid electrolyte interface (SEI) layer.[9,10] The SEI layer on graphite has been directly observed and quantitatively analysed via *in situ* electrochemical atomic force microscopy (AFM).[11] The above techniques reveal many aspects of structural modification that contribute to capacity fading.

The evolution of structural damage in electrodes is the key aspect for capacity fading of Li-ion batteries. It occurs at the atomic lattice level, and then cascades upwards in terms of the length scales to nano- and microstructural levels. The investigation of atomic lattice level processes requires intricate reciprocal space methods such as XANES and EXAFS.[12,13] Nano-structural modifications can be visualised in real space using electron microscopy or high resolution X-ray microscopy. X-ray computed tomography allows non-destructive 3D imaging of the interior of battery electrodes, but relies on complex mathematical inversion procedures and may suffer from reconstruction artefacts. *In situ* X-ray tomography has been successfully applied to visualize particle fragmentation at the micron scale that takes place as a consequence of the very large crystal lattice parameter change during lithiation of Sn.[14] In comparison, combining scanning electron microscopy with focused ion beam serial sectioning (FIB-SEM) allows nano-scale 3D visualisation of the structural modifications that take place during charge/discharge cycling. Wilson et al.[15,16] reported successful applications of FIB-SEM reconstruction of solid oxide fuel cell (SOFCs), and demonstrated quantitative

[a] MBLEM, Department of Engineering Science, University of Oxford, Oxford, OX1 3PJ, UK; E-mail: alexander.korsunsky@eng.ox.ac.uk.
[b] Department of Mechanical Engineering, National University of Singapore, Singapore, 117576.
† Current address: University of Texas at Austin, U.S.A.

Electronic Supplementary Information (ESI) available: 3D reconstructions of electrodes after 1st charge and 1st cycle in addition to XRD and SEM observations of Li-rich particles. See DOI: 10.1039/x0xx00000x

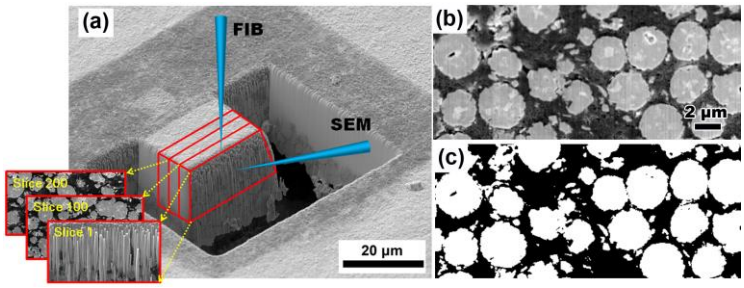

Fig. 1 (a) SEM image showing FIB-SEM configuration and the trench formed within the electrode sample. (b) Cross-sectional SEM image of the fresh electrode after FIB milling, and (c) the corresponding segmented image.

analysis methods for critical microstructural features. In applying this characterization technique in field of LIBs, Wilson,[17] Liu,[18] and Ender[19] independently reported microstructural details of cathodes containing $LiCoO_2$, $LiCoO_2/LiNi_{1/3}Co_{1/3}Mn_{1/3}O_2$ composite, and $LiFePO_4$. However, to the best of our knowledge there have not been published reports that address the changes in the nano-structure as a result of cyclic electrochemical cycling. The information collected inside a battery electrode may help identify the reason for battery degradation, i.e. the loss of Li^+ ion diffusion channels and/or loss of internal electron conductivity. Such loss of conductivity has been attributed to several reasons: the growth of solid electrolyte interface SEI layers, particle collapse, gas generation, loss of contact between composite electrode and current collector, and failure of the binder. Importantly, FIB-SEM tomography data can be used to perform quantitative assessment of various geometric parameters of the electrode, for instance, its porosity, volume fraction, active surface area, particle size distribution, and tortuosity. This information is essential for establishing accurate electrochemical and mechanical models of a particle or an electrode, in order to stimulate the electrochemical response during (de)intercalation of Li, and its mechanical consequences that promote degradation.

Here we report a FIB-SEM serial sectioning and 3D reconstruction of pristine and long-term cycled LIB cathodes containing high-energy Li-rich $Li(Li_{0.2}Mn_{0.54}Ni_{0.13}Co_{0.13})O_2$ (LLNCM) active material. It reveals for the first time that long-term electrochemical cycling leads to fragmentation of particles with spherical morphology. Moreover, the effect is found to vary along the Li^+ diffusion direction into the depth of the cycled electrode from its surface. The large secondary particles of active material composed of the sintered primary grains change their shape significantly as a consequence of charge/discharge cycling. The observed evolution of particle shape away from the initial spheroidal is caused by large scale mass transport and fragmentation. Large numbers of internal voids and cracks were generated between primary grains. This, together with the incomplete reversibility of phase transformation led to the amorphisation of the primary grains and significant volume change of the electrode. Geometric parameters based on quantitative analysis are identified that allow the quantification of the damage process.

Experimental

Preparation of $Li(Li_{0.2}Mn_{0.54}Ni_{0.13}Co_{0.13})O_2$ particles

Spherical $Li(Li_{0.2}Mn_{0.54}Ni_{0.13}Co_{0.13})O_2$ particles were synthesized by a traditional carbonate-assisted co-precipitation method.[30] In a typical process, an aqueous solution containing metal sulphates in a molar ratio of Mn : Ni : Co = 0.54 : 0.13 : 0.13 was firstly prepared. Then, this solution was slowly dripped into an as-prepared NH_4HCO_3/Na_2CO_3 solution with continuously stirring at pH = 8, T = 60°C to obtain the $(Mn_{0.54}Ni_{0.13}Co_{0.13})(CO_3)_{0.8}$ precursor. The precursor was dried overnight at 80°C followed by mixing with Li_2CO_3 powders (5 % excess). Finally, the mixture was fired at 600°C for 10 h and then at 800°C for 15 h to obtain the final product. The corresponding XRD pattern and SEM images are shown in Fig. S1.

Electrochemical cycling

The galvanostatic charge/discharge cycling tests were accomplished in a half battery cell using CR2016-type coin cell. Firstly, the electrode slurries were prepared by mixing active $Li(Li_{0.2}Mn_{0.54}Ni_{0.13}Co_{0.13})O_2$ particles, carbon black (Super P) and polyvinylidene fluoride (PVDF) in a weight ratio of 8 : 1 : 1 with n-methyl-2-pyrrolidone (NMP) solution. The well-mixed slurries were pasted onto Al foil and dried overnight under vacuum at 120°C before assembly. A half battery cell was carefully prepared in a glove-box using the as-prepared cathode, pure Li foil as anode, two pieces of separator (Celgard 2500), and a few drops of electrolyte (1M $LiPF_6$ in EC: DEC = 1 : 1 organic solutions). Four battery cells were charged/discharged over different numbers of cycles using a Neware Battery Test Station [NEWARE Co. Ltd., Shenzhen, China] under a fixed current density of 50 mA g^{-1} between 4.8 V and 2.0 V (vs. Li+/Li). The first battery was charged once to 4.8 V. The second battery was charged once, and then discharged fully to 2.0 V. The third and fourth cells were cycled 15 and 50 times, respectively, and both then left in a fully discharged state. The cycled battery cells were carefully disassembled inside a glove-box. Cathodes were washed using dimethyl carbonate (DMC) three times, and then dried at 80°C in a vacuum oven overnight before FIB-SEM characterization.

FIB-SEM tomography

A fresh electrode and cycled electrodes were studied by serial sectioned using FIB-SEM instrument LYRA3 XM (Tescan s.r.o., Brno, Czech Republic). Thin layers of material were removed by FIB milling from the exposed surface towards the inner part, followed by SEM imaging of each newly exposed surface. As a result, a series of consecutive SEM images with good contrast were obtained, providing input for 3D reconstruction. The pixel size of the SEM images was 50 nm, and the slice thickness was also set to be 50 nm. The image alignment, cropping, and segmentation were accomplished using ImageJ and several plugins. As concluded by Joos et al.[31] and Liu et al.[18], accurate segmentation of 2D images could be best achieved via thresholding by Otsu algorithm.[32] It is important to note the challenge of distinguishing between non-oxide components

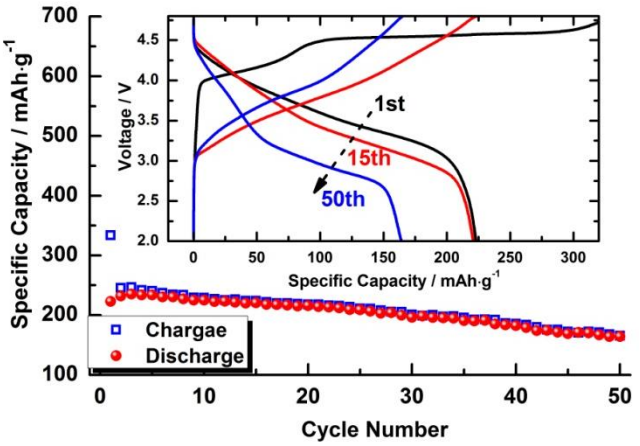

Fig. 2 Cycle performance and corresponding charge/discharge curves of LLNCM electrode at various cycling stages, i.e. 1st, 15th and 50th cycle. Testing condition: 2.0 – 4.8 V, 50mA·g^{-1}, 25°C.

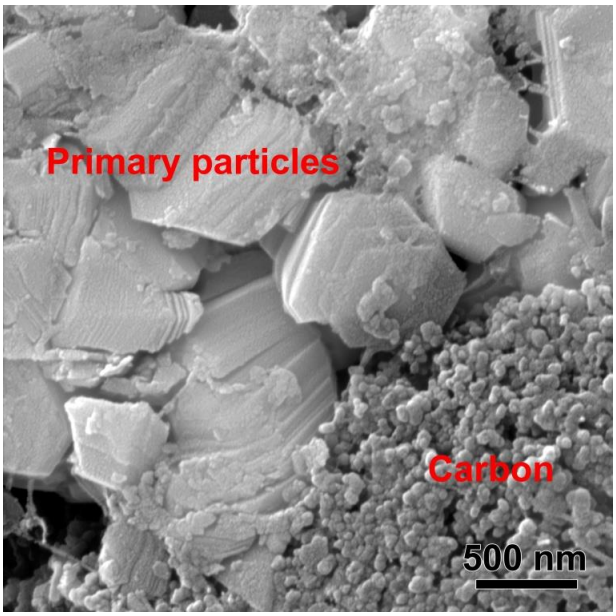

Fig. 3 High magnification SEM image of primary particles of active material that reveals the details of their morphology. Hexagonal habit platelets of oxides can be clearly recognised in the small stack to the top right of image centre, whilst elsewhere the multi-layer nature of the particles composed of laminae ~50 nm in thickness.

(carbon black, polymer matrix, and decomposition products that form during cycling), on the one hand, and the pores present in the cross-section images, on the other. The images forming the series were "stacked" to obtain 3D reconstructions. Five 3D reconstructions were obtained that related to the different electrode cycling stages.

Results and discussion

Cycling performance visualization

Fig. 1 shows a typical FIB milling configuration after preparing a trench to expose the volume of interest (VOI), milling sequence, and a typical SEM image along with the corresponding binary image. All slices selected were relatively

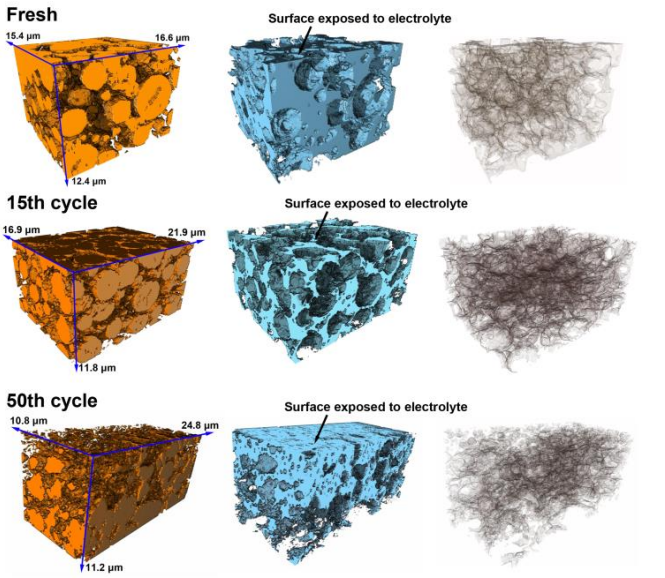

Fig. 4 3D reconstructions of electrodes at various cycling stages, in terms of active LLNCM particles (left), porosity with carbon black and all other non-active materials (middle), and the interface between them (right).

similar to each other in terms of the information they reveal about the composite structure. The slice location within the milling sequence from the VOI surface and into the bulk regions is illustrated from Fig. 1. Fig. 2 shows a typical cycle performance and corresponding charge/discharge curves of LLNCM cathodes. In the first cycle, the LLNCM-based batteries were capable of storing 333 mAh·g^{-1} during charging, and releasing 223 mAh·g^{-1} during discharge. The coulombic efficiency of 67 % was achieved at the current density of 50 mA·g^{-1}. The high reversible capacity and the relatively low coulombic efficiency are typical for lithium-rich layered cathodes, and can be attributed to the activation and partial reinsertion of Li that takes place in the Li_2MnO_3 component of the mixed oxide electrode[20] . After 50 cycles, only 164 mAh·g^{-1} discharge capacity could be delivered where the charge/discharge curves significantly change in shape. The well-known reason for this curve change is the so-called spinel transformation upon cycling, involving transition metal migrations and consequent environmental change of Li during (de)intercalation.

The spheroidal secondary LLNCM grains are composed of primary particles with sharp edges. Fig. 3 illustrates their morphology. This high magnification SEM image reveals the hexagonal habit platelets of oxides that can be clearly recognized in the small stack found to the top right of image centre and viewed at an aspect nearly normal to the plate surface. Elsewhere in the image, the multi-layer nature of the particles is seen closer to edge-on aspect, that shows the particles are composed of laminae ~50nm in thickness. This view suggests that significant anisotropy of thermal, mechanical and diffusional properties between primary particles. As a consequence, their agglomerates are likely to experience significant internal strains and stresses during thermo-mechanical and chemical processes associated with Li

ion intercalation and de-intercalation. This observation provides a conceptual basis for formulating continuum-based

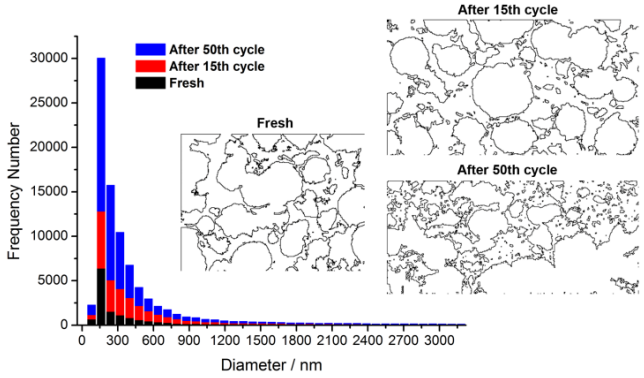

Fig. 5 Particle size distribution diagram showing progressive increase in the number density of smallest particles as a consequence of charge cycling. Insets show particle outline plots, revealing the interfaces between active material particles, on the one hand, and the matrix and voids, on the other. Progressive increase in the number of small particles scattered within the matrix is accompanied by the noticeable gradual decrease in the average size of large particles.

models for modeling damage and degradation in these systems. We now turn our attention to FIB-SEM serial sectioning nano-tomography results at the level of composite consisting of the carbon-loaded polymer matrix material containing secondary particles of active material. The morphological changes observed in the composite during charge/discharge cycling lead to clear distinction being made between fresh, once charged, once cycled, and 15 times cycled electrodes. To obtain a clear perception of the multi-scaling, hierarchical nature of the deformation and damage processes occurring within the composite electrode, we draw on both the 2D microscopic imaging and nano-tomographic information. Detailed examination of SEM image sequences reveals that the highly crystalline primary particles of the type seen in Fig. 3 prior to cycling disappear after 50 cycles, although the spherical morphology of the secondary particles is still apparent. More information inside individual secondary particles has been revealed by FIB-SEM tomography, and is presented and interpreted in the following section. 3D reconstruction of the internal structure of electrodes is best appreciated when rendered electronically using computer software, or viewed as a video (see Supplementary Material). Snapshots from the sequence are shown in Fig. 4 for illustration. In these images, particles of active LLNCM material are represented on the left as bonded yellow solid spheroids, whilst the matrix continuum containing carbon black, binder, pores, decomposed products from electrolyte, etc. is indicated in the second column in light blue. Perhaps the most important discovery reported in this study is the evident fragmentation of the initial spherical LLNCM particle into small sub-micron pieces. This effect is particularly evident after 50 cycles. It is also worth noting that this effect is not uniform with the depth into electrode – an observation that has been recorded consistently from one electrode sample to another in tomographic reconstructions. This effect is revealed in movies S1, S2 and S3 provided as Supporting Material which give additional structural information about the internal structure of these electrodes recorded fresh, and after 15th and 50th cycles, respectively.

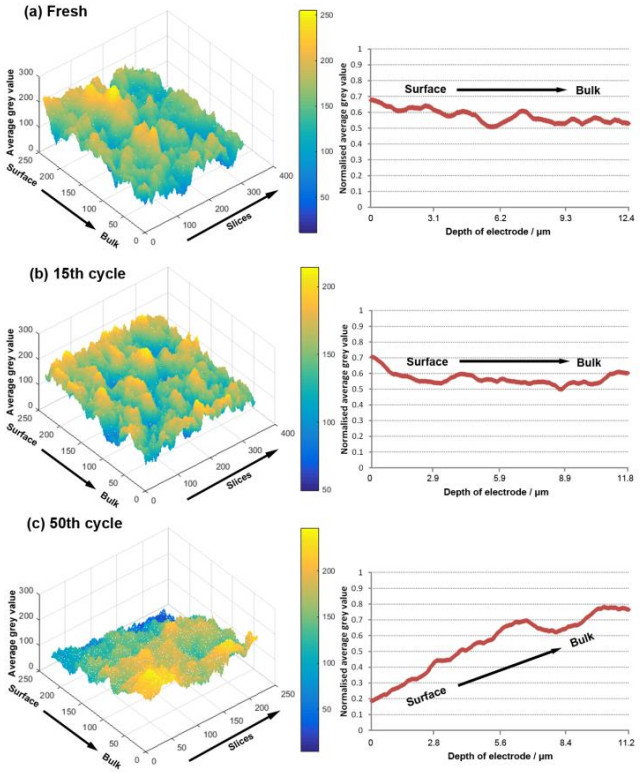

Fig. 6 3D surface plots and 2D projections of (a) fresh, (b) after 15 cycles (c) after 50 cycles, using average grey value based on series of cross-sectional SEM images from cycled electrodes, showing a significant difference in average grey value from surface to bulk regions of electrode after 50 cycles.

The reason the interface in 50-cycle electrode looks 'sparser' is due to the smaller apparent volume of fragmented pieces of active particles: some fragments formed are so fine that they fall below the lower bound of the image resolution. Zheng et al.[21] recently reported observable evidence of fragmented pieces at the surface of lithium-rich particles after extended cycling, using STEM and EELS. Our results provide further, additional solid evidence of fragmented pieces peeled off from initial spherical particles. The intrinsic mechanism that causes such fragmentation is associated with cyclic variation of stress and strain caused by the lattice expansion and contraction due to Li^+ ion concentration changes and gradients that arise during cycling. The underlying mechanism that is ultimately responsible for fragmentation can be referred to as "electrochemical fatigue", because it is associated with the mechanical consequences of charge carrier diffusion. This is discussed in the modeling section below. Here we note that the consequence of this process manifests itself in the interface between the active particles and inactive components becoming less immediately apparent in the images of 50 times cycled electrode in comparison with the fresh one, revealing the progressive erosion of the spherical morphology of LLNCM particles.

Quantitative Particle Size/Volume Fraction Analysis

The availability of detailed 3D information about active material particles allows detailed analysis of their size

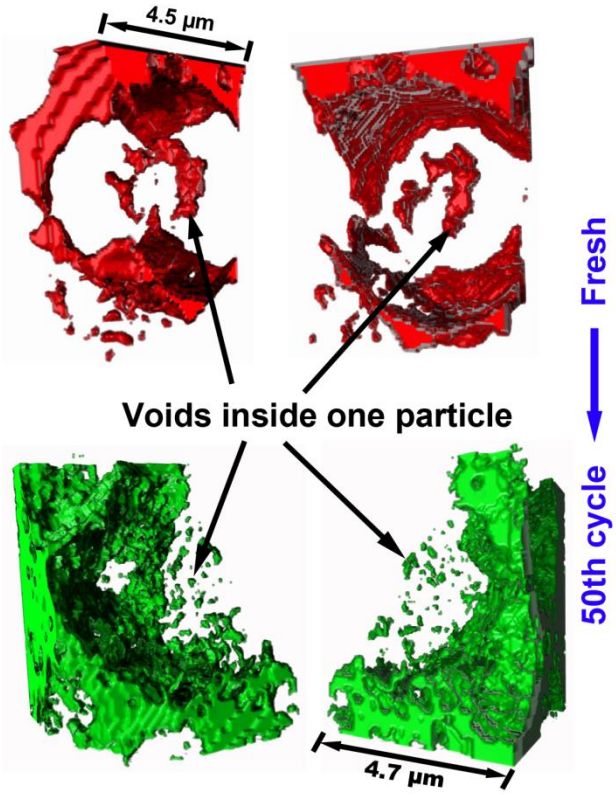

Fig. 7 3D reconstructions of single particles (a) before and (b) after cycling, revealing a continuous void within the particle in the as-prepared state following sintering, and the dispersion of small voids found within the particle the experienced multiple charge cycles.

distribution, and its variation with cycling and position within the electrode. To obtain insight into the processes of particle fragmentation during cycling, we propose the following two statistical measures. Firstly, consider the histogram of particle size distribution shown in Fig. 5. The apparent increase in the number of particles falling into the smallest size range provides direct evidence of particle fragmentation, with large numbers of smaller particles appearing at the expense of the large ones. Whilst revealing the increase in the number of smallest particles using statistical means is straightforward, the corresponding changes at the large particle size end of the distribution presents more of a challenge, since such changes involve small numbers of particles and hence do not appear prominently in the histogram. Instead, we propose to consider the particle outline plots shown in the insets of Fig. 5. The progressive increase in the scattered small particle distribution within the matrix is apparent, as is also the gradual decrease in the average large particle size. This is accompanied by the visible increase in the interfacial boundary length. The boundary presents a barrier to diffusion, thus reducing the battery charging capacity.

The overall volume fraction of the active components was calculated as 57.60% of total volume in the fresh electrode. After 15th cycle, the value changes to 56.68%, and subsequently changes further to 55.01% after 50 cycles of charge/discharge. Note that although these three electrodes were different samples to be cycled, they were prepared by

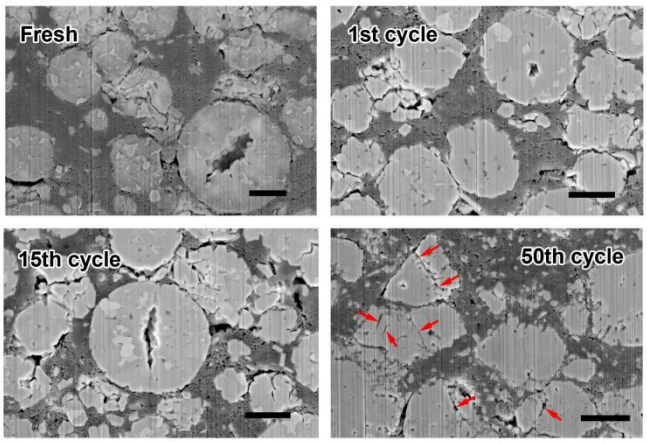

Fig. 8 Cross-sectional SEM images of electrodes at various cycling stages: fresh, after 1st cycle, after 15th cycle, and after 50th cycle. Comparison of the images shows both microscopic damage mechanisms at work, i.e. progressive internal particle voiding and cracking accompanied by the exfoliation and flaking of active material from the surface of secondary particles. The scale bar is 2 µm.

the same well-mixed slurry, with sufficient care taken to exclude the possibility of preparation-induced variation in the volume fraction. In addition to volume fraction evolution, there are further significant structural changes taking place with cycling. Fig. S2 shows the 3D reconstruction of electrodes after the 1st charge, and after the full 1st cycle. Although the overall volume fraction change of active material comparing the 50th cycled to the fresh ones is only 2.6 %, this change is sufficiently significant to correlate it with the gradual capacity fading as a result of charge/discharge cycling. It is speculated that two reasons might be responsible for this reduction of the active material volume fraction. The first one is the possible growth of pores and decomposed products of electrolyte. The second one is likely to be the well-known "corrosion" effect related to the dissolution of transition metals (Co, Ni, and Mn).[5-7] It has been reported that transition metal ions could be found on the surface of the counter electrode, which implies that they have undergone migration through the battery assembly. Thus, particle dissolution upon deep cycling contributes to the reduction of volume fraction of the active components.

The variation of the volume fraction of active component in the depth direction of the electrode was also calculated in a statistical measure and shown in Fig. 6. 3D surface plots of the average grey value were made at different FIB milling depths that were interrogated in the course of FIB-SEM tomographic data collection, illustrated in Fig. 6. The grey value for black is 0, indicating inactive components. The grey value for white is the range maximum of 255, and corresponds to the brightest regions of LLNCM particles. Therefore, the higher the average grey value, the larger is the volume fraction of active components. While the volume fraction calculation over the entire 3D reconstruction of the studied tomographic region of interest represents complete volume averaging, the analysis

illustrated in Fig. 6 is related to the variation of the volume fraction of active material along the depth direction into the

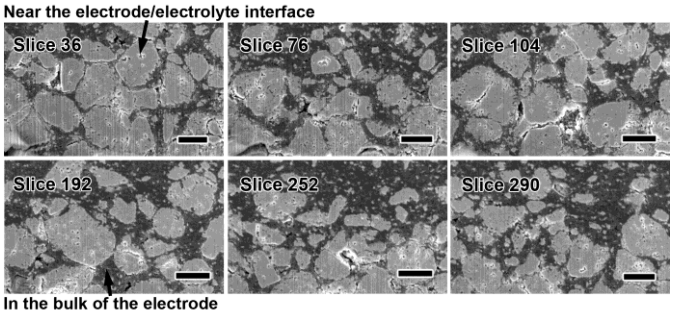

Fig. 9 A sequence of cross-sectional SEM images of 50th cycled electrode starting close to VOI surface and progressing into the bulk. The common observation concenrs the presence of internal voids and cracks grown within particles. The scale bar is 2 µm.

electrode. In the fresh and 15 times cycled electrodes the variation of the volume fraction from material surface into the bulk is not immediately apparent. This conclusion is strongly supported by the line plots obtained by averaging the intensities from the same depth data in all slices. A different volume fraction profile is seen in the electrode subjected to 50 cycles. A significant variation of the volume fraction can be readily recognized between surface and bulk regions. The result suggests that a smaller amount of active LLNCM material persists in the near surface regions compared to bulk. This observation can be correlated with the accelerated diffusion of Li+ through the electrolyte to the electrode surface regions, resulting in the faster local effective charge rate. We conclude from these observations that progressive capacity fading of the Li-rich cathode is likely to be associated with spatially inhomogeneous particle fragmentation that is accompanied by the reduction in the amount of active material within the electrode available for lithium storage during extended cycling.

Particle Fragmentation visualization

To investigate further the fragmentation mechanisms of the LLNCM active material within Li-ion battery cathode, two particles with the dimensions of about 3~5µm were identified in the material examined before and after extended cycling. The nano-tomography reconstructions of the two particles are shown in Fig. 7. To aid the purpose of visualising the spatial distribution of damage within the particles, the active material forming the two particles was rendered transparent, while the inner voids and the associated inactive material components are solid in solid colour. The rendered image based on the data collected prior to cycling shows the presence of a single, large, continuous void within the particle that is known to be principally associated with the high temperature sintering process. It occurs during cooling down of the material from the 800°C sintering temperature to room temperature. The outer skin of the spheroidal particle cools down first, leading to strengthening of the spherical shell ahead of the warmer core. Upon further cooling the core ends up being subjected to hydrostatic tension. The significant tensile stress present in the core may be released either by spherical voiding, or by preferential planar cracking that leads to the release of one particular stress component. Deng et al.[22] and Koenig et al.[23]

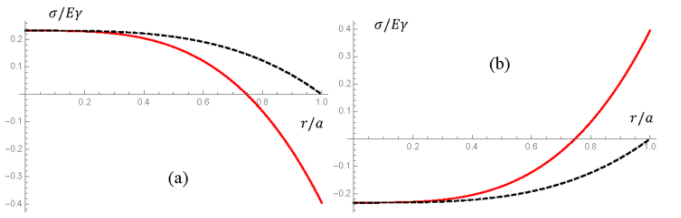

Fig. 10 A snapshot of the internal stress profiles (normalised by the value $E\gamma$, where E denotes Young's modulus of active material, and γ the equivalent lattice strain caused by complete lithium deintercalation) predicted by transient diffusion and eigenstrain model.[28] The profiles are shows at normalised time $\tau = Dt/a^2 \cong 0.03$ after the beginning of fast (a) charging and (b) discharging of the battery. The spheroidal particle of active material is assumed to have radius *a*, and the diffusivity of Li+ is denoted by D. The radial stress component is plotted using black dashed line, and hoop stress the red solid line.

reported similar observations of inner voids and/or cracks within Li-rich particles synthesized by carbonate-assisted co-precipitation and subjected to sintering at 900°C. The route for this stress release process may vary between particles, as confirmed by our observation of multiple tomographic reconstructions of individual particles.

Let us now compare the initial state of the particle prior to charging with its appearance following long-term cycling. A large population of small nano-scale voids is clearly visible inside the cycled particle of LLNCM material. This phenomenon was observed almost in each particle located in the zone of reduced active material content within the cycled electrode. We surmise that that the phenomenon of nano-voiding is related to inner stressing and fatigue damage accumulation during cycling. Fig. 8 shows a series of cross-sectional SEM images of the electrode after 50 cycles to substantiate the observation of the dispersion of voids within most particles of active material. It can be speculated that two reasons may be responsible for the appearance of small voids. The first route can be ascribed to phase transformation occurring during lithiation/delithiation. Gu et al.[24] proposed a possible mechanism of spinel formation in separated Li_2MnO_3 and $LiMO_2$ components linked to the migration of transition metals into lithium layers, oxygen release, and subsequent nucleation and growth of spinel domains. Complex local phase transformations result in the misfit strain between crystal lattices of the original and transformed phases even within a single crystal. Following repeated lithiation/delithiation process, the misfit strain causes the proliferation of defects and ultimately the appearance of voids within individual polycrystalline particles. The second route that we wish to consider is the consequence of Li^+ transient diffusion during charging (particularly at fast rates) that leads to the generation of differential expansion and stress gradient at two distinct scales. On the one hand, gradients arise at the *macroscopic scale* between the electrode surface exposed to electrolyte and the bulk regions of the electrode.[25] On the other hand,

steep expansion gradients arise at the *microscopic scale* between the surface of each individual LLNCM spheroidal particle and its core.[26]

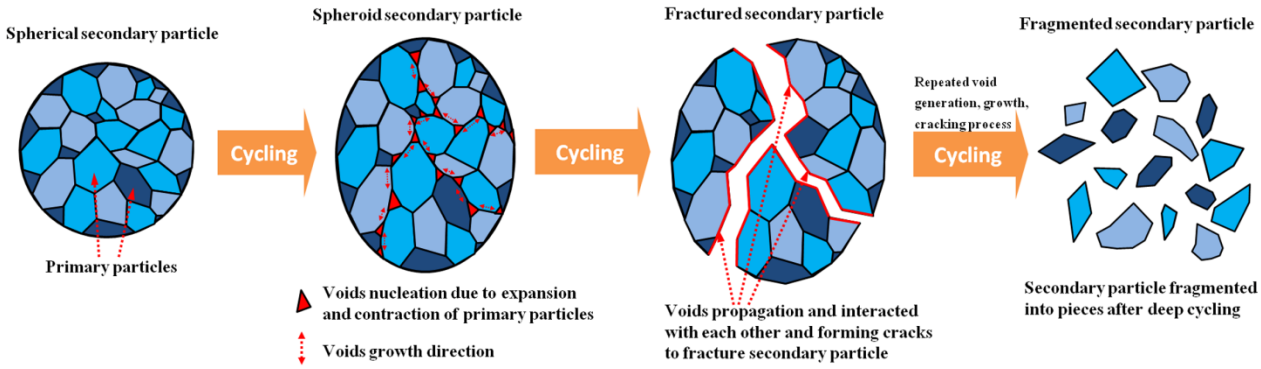

Fig. 11 Schematic illustration of fragmentation mechanisms of Li-rich particles upon deep cycling.

Direct evidence of the particle fragmentation mechanisms described above being at work in Li-ion battery cathodes can be found in Fig. 9. Note that the slice sequence as numbered from 36 to 290 is as same as the one described in Fig. 1, in which it provides the similar information in terms of composite structure and fragmented particles. In each of the slice image, upper region is near the electrode/electrolyte interface while the lower region is in the bulk of the electrode. Cross-sectional SEM images allow the following observations to be made, and deductions to be drawn.

1) Large inner voids could be observed in some particles after 15th cycle.

2) Some of the broken particles that display sharp crystal edges are likely to be a consequence of the electrode compaction during preparation, rather than electrochemical "grinding".

3) The morphology of spherical secondary particles could be maintained after 15th cycle, while it changes significantly to assume irregular shapes after the 50th cycle.

4) The sharp edges of polygonal particles are likely to arise due to the initiation of internal cracks causing surface peeling of original particles. Cracks initiating within particles are clearly seen, as pointed out by the arrows in Fig. 9.

5) The cracks are likely to be the consequence of internal voiding.

6) Once a large particle fragments into two pieces because of crack growth, the two resulting pieces follow a similar fracture route to form even smaller fragments. Due to the differences in the concentration of Li^+ ions *and* the variation in the maximum concentration gradient with the depth of electrode, the extent of fragmentation along this direction varies. Combined, the above mechanisms lead to the structural alterations observed in the 50th cycled electrode shown in Fig. 4.

Particle Fragmentation Modeling

Stress development at the macro-scale of battery electrodes is highly sensitive to the charge rate. An abrupt change of lithium concentration at cathode surface causes high local gradient that propagates into the electrode, creating local microscopic conditions that vary in their severity with distance from the surface. Consideration of the classical macro-scale solution of the transient diffusion equation[27] reveals that the maximum concentration gradient experienced by the particles of active material at the microscopic scale decays as a function of distance from the surface. This suggests that the microstress evolution within the particles follows a similar scenario throughout the electrodes, but the variation in the rate and magnitude of local concentration changes suggests that near surface regions sustain cyclic damage ahead of the bulk layers.

Let us now consider at the microscopic scale the cyclic lattice straining caused by the Li ion transient diffusion through the cathode material. This phenomenon can be thought of as the principal cause of progressive material fragmentation that ultimately results in material degradation and battery capacity fading. For the purposes of the present study we utilize micro-scale analysis framework of the recently published model devoted to the effect of Li ion transient diffusion on the internal stress within spheroidal secondary particles of active material.[28] The model was constructed by combining the solution of transient diffusion equation with the equations of continuum elasticity perturbed by the presence of eigenstrain due to lithium intercalation.

Fig. 10 illustrates the principal conclusions of the diffusional micro-stress model used in further reasoning. In the course of battery charging illustrated in Fig. 10(a), the volumes of active material lying on the periphery of the spheroidal secondary particle undergo expansion, causing the development of compressive hoop stress. This is balanced by the appearance of tensile stress at the core. It is important to note that the model predicts this tensile stress state to be hydrostatic and significant in magnitude, reaching the peak value of $\sigma \cong E\gamma/3$. Taking the typical Young's modulus value for active material of 280 GPa,[29] and the complete lattice expansion strain of 0.035 gives an estimate of the maximum hydrostatic stress at particle core of ~3.3 GPa. Such stress values clearly in excess of the tensile strength of active material could be reached under fast charging condition, resulting in internal cracking and voiding that propagate outwards from the particle core. The occurrence of stresses even as low as 20% of this value repeatedly and at elevated temperatures, as e.g. during

battery charge cycling, is likely promote internal damage by the combined creep and fatigue mechanism, resulting in distributed damage. Fig. 10(b) contains plots that provide the stress state snapshot during fast battery discharge. In contrast with Fig. 10(a), the particle core finds itself under hydrostatic compression. However, the particle periphery experiences shear stress that in the extreme case also amounts to values as high as $E\gamma/3$. Therefore, at this phase of battery charge cycling damage is likely to be sustained in the form of material fragmentation and exfoliation at the surface of the secondary particle.

Conclusions

Following the findings presented above, the fragmentation mechanisms of Li-rich particles can be summarized and schematically illustrated in Fig. 11.

1) High temperature sintering usually leads to the formation of a single large continuous void at the centre of a secondary particle, due to temperature gradients that arise during cooling.

2) During electrochemical cycling the primary particles experience a large volume expansion/contraction strain due to lithiation/delithiation. The inhomogeneity and anisotropy of the primary particles leads to the nucleation and growth of numerous small voids within them (Fig. 7). These voids are randomly distributed inside the secondary particles.

3) Upon deep cycling, discontinuous voids propagate, interact and link to become cracks (Fig. 9).

4) When the cracks propagate across an entire secondary particle, it fragments into two. This fragmentation scenario continues to repeat itself, resulting in the diminution of secondary particles and the change in their morphology that reveals the preponderance of fractured sharp-edges (Fig. 9).

5) At the electrode surface that experienced full electrochemical activation, such fragmentation is found to be more severe than in the bulk area of electrode. This is confirmed by the variation of particle sizes with depth after 50^{th} cycle, as seen in Fig. 6.

6) The Fragmentation increases the surface area of the particles, which may contribute to the accelerated dissolution and transport of transition metals through the electrolyte, that is evidenced by the apparent reduced volume fraction of active materials.

7) Numerical modelling of diffusion and stress shows that the initiation and propagation of small voids may be explained by considering the stress states that arise due to concentration gradients of Li, and that depend strongly on the charge rate.

This study reports the feasibility of utilizing FIB-SEM to reconstruct 3D structure of electrode before and after extended electrochemical cycles. Using Li-rich $Li(Li_{0.2}Mn_{0.54}Ni_{0.13}Co_{0.13})O_2$ cathode, for the first time it was found that the spherical particles experience an inevitable fragmentation process to form small pieces of particles during deep cycling, while the fragmentation extent varies along the depth direction of electrode. In addition, reconstructions of the as-prepared and cycled particles revealed a large amount of voids generated inside cycled particle because of repeated lithiation/delithiation process. Furthermore, a possible fragmentation mechanism and a theoretical model were established to help understanding these observations. These observations indeed provide several possible reasons to explain the mechanisms of capacity fading in such Li-rich layered cathodes. 1) The reduced volume fraction of LLNCM upon cycling implies decreased amount of active Li host structure. 2) The increased surface area of active particles as a result of particle fragmentation experiences severer corrosion from electrolyte at high charging states. 3) The internal stress due to particle fragmentation leads to the loss of close contact between active particles and carbon black. This FIB-SEM 3D reconstruction provides an effective approach to explore new insights of all-types of cycled electrodes. The nearly-perfect reinstatement of local structure of composite electrode, in addition to the detailed quantitative information obtained is constructive for understanding the complex degradation mechanisms of electrodes for lithium ion batteries.

Acknowledgement

AMK acknowledges funding received for the Multi-Beam Laboratory for Engineering Microscopy (MBLEM) at Oxford through EU FP7 project iSTRESS (604646), and the provision of facilities at the Research Complex at Harwell (RCaH) for the Centre for In situ Processing Studies (CIPS).

Notes and references

1 A. Ito, D. C. Li, Y. Sato, M. Arao, M. Watanabe, M. Hatano, H. Horie, Y. Ohsawa, *Journal of Power Sources,* 2010, **195**, 567.
2 H. J. Yu, R. Ishikawa, Y. G. So, N. Shibata, T. Kudo, H. S. Zhou, Y. Ikuhara, *Angewandte Chemie-International Edition*, 2013, **52,** 5969.
3 M. Gu, A. Genc, I. Belharouak, D. P. Wang, K. Amine, S. Thevuthasan, D. R. Baer, J. G. Zhang, N. D. Browning, J. Liu, C. M. Wang, *Chemistry of Materials*, 2013, **25,** 2319.
4 A. Boulineau, L. Simonin, J. F. Colin, C. Bourbon, S. Patoux, *Nano Letters***,** 2013, **13,** 3857.
5 G. G. Amatucci, J. M. Tarascon, L. C. Klein, *Solid State Ionics,* 1996, **83,** 167.
6 K. Amine, Z. H. Chen, Z. Zhang, J. Liu, W. Q. Lu, Y. Qin, J. Lu, L. Curtis, Y. K. Sun, *Journal of Materials Chemistry*, 2011, **21,** 17754.
7 B. H. Song, Z. W. Liu, M. O. Lai, L. Lu, *Physical Chemistry Chemical Physics*, 2012, **14,** 12875.
8 J. H. Lee, J. K. Hong, D. H. Jang, Y. K. Sun, S. M. Oh, *Journal of Power Sources*, 2000, **89,** 7.
9 D. Aurbach, B. Markovsky, I. Weissman, E. Levi, Y. Ein-Eli, *Electrochimica Acta,* 1999, **45,** 67.
10 J. Shim, R. Kostecki, T. Richardson, X. Song, K. A. Striebel, *Journal of Power Sources*, 2002, **112,** 222.
11 A. von Cresce, S. M. Russell, D. R. Baker, K. J. Gaskell, K. Xu, *Nano Letters*, 2014, **14,** 1405.
12 X. Q. Yu, Y. C. Lyu, L. Gu, H. M. Wu, S. M. Bak, Y. N. Zhou, K. Amine, S. N. Ehrlich, H. Li, K. W. Nam, X. Q. Yang, *Advanced Energy Materials*, 2014, 4.
13 J. R. Croy, M. Balasubramanian, D. Kim, S. H. Kang, M. M. Thackeray, *Chemistry of Materials*, 2011, **23,** 5415.

14 M. Ebner, F. Marone, M. Stampanoni, V. Wood, *Science*, 2013, **342,** 716.
15 J. R. Wilson, M. Gameiro, K. Mischaikow, W. Kalies, P. W. Voorhees, S. A. Barnett, *Microscopy and Microanalysis*, 2009, **15,** 71.
16 J. R. Wilson, W. Kobsiriphat, R. Mendoza, H. Y. Chen, J. M. Hiller, D. J. Miller, K. Thornton, P. W. Voorhees, S. B. Adler, S. A. Barnett, *Nature Materials,* 2006, **5,** 541.
17 J. R. Wilson, J. S. Cronin, S. A. Barnett, S. J. Harris, *Journal of Power Sources* 2011, **196,** 3443.
18 Z. Liu, J. S. Cronin, Y. C. K. Chen-Wiegart, J. R. Wilson, K. J. Yakal-Kremski, J. Wang, K. T. Faber, S. A. Barnett, *Journal of Power Sources,* 2013, **227,** 267.
19 M. Ender, J. Joos, T. Carraro, E. Ivers-Tiffee, *Electrochemistry Communications*, 2011, **13,** 166.
20 B. H. Song, M. O. Lai, L. Lu, *Electrochimica Acta,* 2012, **80,** 187.
21 J. M. Zheng, M. Gu, J. Xiao, P. J. Zuo, C. M. Wang, J. G. Zhang, *Nano Letters*, 2013, **13,** 3824.
22 H. X. Deng, I. Belharouak, R. E. Cook, H. M. Wu, Y. K. Sun, K. Amine, *Journal of the Electrochemical Society*, 2010, **157,** A447.
23 G. M. Koenig, I. Belharouak, H. X. Deng, Y. K. Sun, K. Amine, *Chemistry of Materials,* 2011, **23,** 1954.
24 M. Gu, I. Belharouak, J. M. Zheng, H. M. Wu, J. Xiao, A. Genc, K. Amine, S. Thevuthasan, D. R. Baer, J. G. Zhang, N. D. Browning, J. Liu, C. M. Wang, *Acs Nano*, 2013, **7,** 760.
25 K. J. Zhao, M. Pharr, J. J. Vlassak, Z. G. Suo, *Journal of Applied Physics*, 2010, 108.
26 K. J. Zhao, M. Pharr, S. Q. Cai, J. J. Vlassak, Z. G. Suo, *Journal of the American Ceramic Society*, 2011, **94,** S226.
27 A. N. Tikhonov, A. A. Samarskiĭ, *Equations of Mathematical Physics*, Courier Corporation, **1990**.
28 A. M. Korsunsky, T. Sui, B. H. Song, *Materials & Design*, 2015, In press.
29 L. M. Wu, W. H. Lee, J. Zhang, *Materials Today: Proceedings*, 2014, **1,** 82.
30 L. Li, Y. L. Chang, H. Xia, B. H. Song, J. R. Yang, K. S. Lee, L. Lu, *Solid State Ionics* 2014, **264,** 36.
31 J. Joos, T. Carraro, A. Weber, E. Ivers-Tiffee, *Journal of Power Sources* 2011, **196,** 7302.
32 N. Otsu, Ieee Transactions on Systems Man and Cybernetics 1979, 9, 62.

Journal of Materials Chemistry A

ARTICLE

Graphical Table of Contents

This study reports the feasibility of utilizing focused ion beam-scanning electron microscopy sectioning to reconstruct 3D structure of electrode before and after extended electrochemical cycles. Serious fragmentation of Li-rich layered spherical particles is observed and investigated. This is speculated to be one possible reason for the capacity fading in this system.

Keywords: FIB-SEM tomography, lithium-rich layered cathode, eigenstrain modelling, lithium-ion batteries

Title: Nano-structural changes in Li-ion battery cathode during cycling revealed by FIB-SEM serial sectioning tomography